Effects of Cr Concentration on Cementite Coarsening in Ultrahigh Carbon Steel

MATTHEW D. HECHT, YOOSUF N. PICARD, and BRYAN A. WEBLER

Ultrahigh carbon steels (UHCS) containing 1 wt pct Cr (1Cr UHCS) were heat treated at 1073 K, 1173 K, or 1243 K (800 °C, 900 °C, or 970 °C) for durations of 5 minutes up to 24 hours to study cementite coarsening. Results were compared to a previous study on coarsening of a UHCS with 4 wt pct Cr (4Cr UHCS) and significantly different behavior was observed. In the heat-treated 1Cr UHCS, particles clustered in zones that were tens of microns near branches of the cementite network. The opposite trend was observed in the 4Cr UHCS, in which the regions within a few microns near the cementite network were entirely denuded of particles. Causes for differences in coarsening behavior in 1Cr and 4Cr UHCS are discussed.

https://doi.org/10.1007/s11661-019-05403-w

I. INTRODUCTION

ULTRAHIGH carbon steels (UHCS) are a class of steels containing 1.0 to 2.1 wt pct C. The high carbon content causes precipitation of hard, brittle carbide phases during casting and/or heat-treatment processes. These carbide phases usually form as a network along the prior austenite grain boundaries in the UHCS. The type of carbide depends on the composition; M_3C (cementite), M_7C_3, and $M_{23}C_6$ are the most common carbide phases. The carbide phases increase the surface hardness and wear resistance, properties necessary for forming applications such as shaping or rolling other metals. Thus, UHCS are commonly used as tool steels and in rolling mills. UHCS are typically heat treated to improve mechanical properties or machinability. In the 1970s, researchers found that UHCS could be made superplastic at elevated temperatures after thermomechanical processing.[1] The thermomechanical processing also improved the room temperature toughness of the UHCS,[2] leading researchers to explore UHCS for applications traditionally utilizing lower carbon steels, such as sheet and automotive steels.[3,4]

The heat-treatment processing relevant to the present study is spheroidization, in which the steel is heated near or above the eutectoid temperature. During spheroidization, cementite lamellae in pearlite (an alternating layered structure of ferrite and cementite) transform into equiaxed particles. If heating is continued after spheroidization, carbide particles will undergo curvature-driven coarsening. The rate of coarsening at a given temperature depends on the diffusion mechanism which is dominant during coarsening,[5–9] and the diffusion coefficient of the diffusing species. Both fracture toughness[10] and yield strength[11] are affected by carbide particle sizes; finer particle sizes are usually more beneficial to mechanical properties. However, finer particle sizes are also more likely to cause a divorced eutectoid transformation inhibiting pearlite reformation during cooling.[12] Reforming the pearlite might help increase wear resistance,[13] so a heat treatment that produces larger particles with larger spaces between them might ultimately be more suitable. Understanding the particle coarsening behavior is thus very desirable when designing heat-treatment processes.

This study investigates effects of Cr content on cementite coarsening by administering a series of different heat treatments to an UHCS containing 2 wt pct C and 1 wt pct Cr. This study builds on a previous study in which the authors administered the same series of heat treatments to a 2C-4Cr UHCS.[14] Two phenomena related to particle coarsening were noted during heat treatment of the 2C-4Cr UHCS: (1) *multimodal coarsening* particles on grain boundaries (GB particles) coarsened more quickly than particles within the grains (IG particles), and (2) *denuded zones* regions within a few micrometers of carbide network branches became denuded of particles, increasing in size as a power of the elapsed time. The authors also found that volumetric diffusion was inhibited during coarsening of 2C-4Cr UHCS and hypothesized that Cr was responsible for lowering the effective diffusion coefficient for cementite coarsening. Cr alloying may increase the activation energy of iron self-diffusion[15]; for instance, Zhang *et al.*[16] noted that "the addition of substitutional

MATTHEW D. HECHT, YOOSUF N. PICARD, and BRYAN A. WEBLER are with the Department of Materials Science and Engineering, Carnegie Mellon University, 5000 Forbes Avenue, Pittsburgh, PA 15213. Contact e-mail: Webler@cmu.edu
Manuscript submitted October 24, 2018.
Article published online August 19, 2019

alloying elements (Mn, Si, Cr) can remarkably retard the coarsening of cementite particles'' in a 1 wt pct C steel. Thus, the goal of this study is to investigate the effects of Cr content on cementite particle coarsening and denuded zones.

Previous studies have examined coarsening of cementite particles resulting from two different microstructures: (1) coarsening of cementite produced during tempering of supersaturated martensite[17–19] and (2) coarsening of spheroidized pearlite.[20–22] To the authors' knowledge, the maximum carbon concentration, chromium concentration, and temperature utilized in prior studies of cementite coarsening were 1.4 wt pct C, 1.5 wt pct Cr, and 1013 K (740 °C), respectively. The studies of 2C-1Cr UHCS and 2C-4Cr UHCS extend the range of coarsening studies by utilizing carbon contents and temperatures up to 2 wt pct and 970 °C, respectively. Additionally, the phenomenon of denuded zones during coarsening has not been examined in the past.

II. MATERIALS AND METHODS

The experimental procedures used in this study are very similar to those of our previous study on 2C-4Cr UHCS alone.[14] Some portions of the procedure are unmodified from that study and are reproduced here.

Sections from two different UHCS mill rolls were provided by Miller Centrifugal Casting (MCC). One of the rolls contained 4 wt pct Cr (4Cr), and the other contained 1 wt pct Cr (1Cr). Samples were sent to IMR labs in New York for compositional analysis. Carbon and silicon were measured by combustion-infrared absorbance, and other elements by ICP-AES per ASTM 1090-11. Table I shows the compositions of all samples. Cubic samples approximately 1 cm on each side were cut from the rolls using a water-cooled alumina cutoff wheel. Samples were heat treated in a box furnace at temperatures of 1073 K, 1173 K, or 1243 K (800 °C, 900 °C, or 970 °C) for times of 5, 15, 90 minutes, 3, 8, or 24 hours. Samples were then quenched in water after the heat treatment.

Heat-treated samples were cross-sectioned along their centers with a water-cooled alumina cutoff wheel, then ground using successively finer SiC papers (about one minute per paper gradation), and finally polished with a 1 μm alumina suspension. Polished samples were etched for 25 to 30 seconds in 4 to 5 pct Nital (nitric acid in ethanol). Etched samples were imaged using scanning electron microscopy (SEM, Phillips XL-30 at 20 kV accelerating voltage in secondary electron detection mode) and optical microscopy (OM, Leica series 750). Compositions of different microstructural components were analyzed in the SEM using energy-dispersive X-ray spectroscopy (EDS, Oxford Instruments INCA X-act at 20 kV accelerating voltage and $>$ 10,000 counts per scan). Equilibrium phase compositions and diffusivities were calculated using Thermo-Calc (version 2017a, including DICTRA, using the TCFE9 and MOBFE4 databases).

Table I. Compositions of the UHCS Used in This Study

	Fe	Cr	C	Mn	Mo	Si	Ni
1Cr UHCS	bal.	3.86	2.02	0.68	0.33	0.65	1.45
4Cr UHCS	bal.	0.92	1.89	0.67	0.31	0.77	1.30

Since the heat treatments were conducted in air, decarburized regions were avoided in the microstructural analysis. The greatest potential depth of decarburization for these heat treatments was calculated at about 3 mm for 24 hours at 1243 K (970 °C).[23] All samples were thus sectioned to be more than twice as large as this depth and microstructural characterization was confined to the center of each 1 cm sample.

Lamellar spacing of pearlite in the 1Cr and 4Cr UHCS was measured from SEM micrographs by drawing straight lines in ImageJ within five or more different pearlite colonies in each UHCS sample. Each line was started at the center of one pearlite lath, and then extended perpendicular to that lath until it intersected the center of another lath 4 to 10 μm away within the same pearlite colony. Spacing was determined by dividing the line length by one less than the number of lamellae intersected by the line. This method of determining lamellar spacing does not account for stereology, *i.e.*, the planes of sectioning might not be perpendicular to the orientation of the lamellae. Vander Voort and Roósz described the spacing derived from the method of drawing lines parallel to pearlite lamellae as the ''directed mean lamellar spacing,'' and determined that the ''true mean lamellar spacing'' (spacing of lamellae oriented perpendicularly to the measurement plane) was equivalent to the directed mean lamellar spacing multiplied by $\pi/4$.[24]

Particle size distribution analysis was performed on the OM micrographs using the ImageJ software.[25] Particle areas (A) were measured, and diameters were calculated assuming that $d = 2\sqrt{A/\pi}$. Corrections for stereology were made according to Saltikov's procedure[26]: logarithms of the diameters were taken, then sorted into bins (size classes) of 0.1 log (μm), from $-$ 0.4 (0.4 μm) to 0.8 (6.3 μm). The number of particles measured within each bin, N_{Ai}, was corrected for stereology to N_{vi}, according to the following equation:

$$N_{\mathrm{Vi}} = \alpha_i N_{\mathrm{Ai}} - \sum_{j-1}^{i-1} \alpha_{j+1} N_{A(i-j)}$$

In the above expression, α_i are stereological constants derived by Saltikov that adjust N_{Ai} based on the probability of sorting larger particles into smaller bins due to off-center intersections with the 2D planes of measurement. Errors due to the assumption of perfectly spherical particles should not be significant since the aspect ratios of the particles were not large.[27]

III. RESULTS

A. *SEM*

1. *Initial (as-cast) microstructure*

Before the heat treatment, the as-cast 1Cr and 4Cr microstructure consisted of a cementite network and pearlite matrix. Figure 1 shows the starting microstructure of the 1Cr UHCS (the 4Cr UHCS microstructure, shown in our previous study,[14] was very similar to the 1Cr microstructure). The dark phase in Figure 1(a) (indicated by arrows) is the cementite network that was formed on austenite (γ) grain boundaries during cooling. The as-cast microstructure also sporadically contained some acicular Widmanstätten cementite associated with the cementite network, as shown in Figure 1(b). A pearlite matrix surrounded the cementite network, as shown in Figure 1(c). The directed mean lamellar spacing in the as-cast 4Cr UHCS (0.13 ± 0.02 μm) was about one-third that of the as-cast 1Cr UHCS (0.40 ± 0.08 μm).

2. *Heat-treated microstructure*

Heat treatment caused coarsening of pearlite in both the 1Cr and 4Cr UHCS. However, some microstructural differences were observed between the two compositions after heat treatment. Microstructures of the 1Cr and 4Cr UHCS after heat treating at 1243 K (970 °C) are compared in Figure 2. The four parts of Figures 2(a) through (d) correspond to different heat-treatment durations, ranging from 5 minutes to 24 hours. Each part of Figure 2 is further divided into four sections that show regions within a few tens of microns of the cementite network, and show regions in the matrix about 50 μm away from the network. Two aspects of the heat-treated microstructures differed depending on the composition: (1) In regions near the network, the 1Cr UHCS exhibited particle clustering near the network branches while 4Cr UHCS exhibited denuded zones near the network branches. (2) In the matrix further away from the network, the areal density of particles in the 1Cr UHCS was qualitatively very low compared to the same regions in the 4Cr UHCS.

Representative areas within about 50 μm around branches of the cementite network in the heat-treated 1Cr and 4Cr UHCS are shown in Figure 3. Particle areal densities within these areas were either low or high, and regions of different densities could be distinguished in the micrographs by eye (low-density regions being almost entirely devoid of particles). Black lines in the figure were traced manually along the edges of particles which were judged to be on the boundaries between regions of high and low particle density. The high-density regions were found inside the black lines (adjacent to the cementite network) in the 1Cr UHCS, and outside the black lines (away from the cementite network) in the 4Cr UHCS. Thus, black lines roughly denote the extent of denuded zones in the 4Cr UHCS, and the extent of particle "clustering" near the cementite network in the 1Cr UHCS. In a previous study,[5] the authors found that denuded zone widths exhibited a power-law relation with heat-treating time in the 4Cr UHCS, reaching about 8 μm after 24 hours at 970 °C. No such power-law relation was found in the 1Cr UHCS; clustered zones instead consistently extended about 10 to 20 μm away from the network branches for every heating time.

Heat treating at lower temperatures decreased the differences between microstructures in the 1Cr and 4Cr UHCS. As shown in Figure 4, lowering the heat-treatment temperature in the 1Cr UHCS increased particle areal densities within the matrix away from the vicinity of the network branches. Heat treating at 1043 K and 1143 K (800 °C and 900 °C) did not result in areas within the matrix that were entirely devoid of particles, as had been observed after heat treatment at 970 °C. However, particle clustering was still observed near cementite network branches in the 1Cr UHCS at both 1043 K and 1143 K (800 °C and 900 °C). Denuded zones were never observed in the 1Cr UHCS at any heat-treatment temperatures.

3. *EDS*

Compositions of microstructural components in the 1Cr and 4Cr UHCS were measured in the SEM using EDS. As shown in Figure 5, overall composition was measured using area scans; point scans were utilized to measure compositions of the cementite network, cementite particles, and matrix. The point and area EDS measurements in the 1Cr UHCS are not shown because they were very similar to those shown in

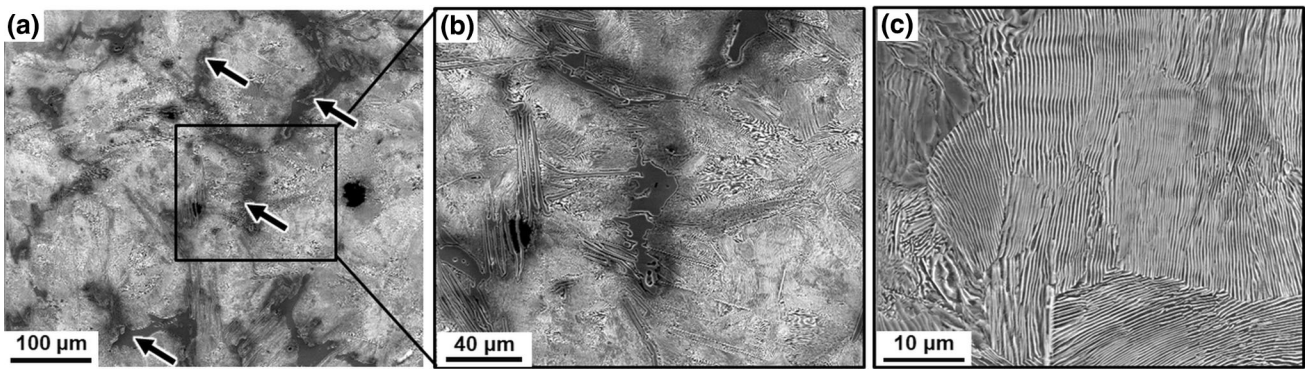

Fig. 1—SEM micrographs of the as-cast microstructure in the 1Cr UHCS showing (*a*) cementite network and matrix, (*b*) acicular Widmanstätten cementite, and (*c*) lamellar pearlite.

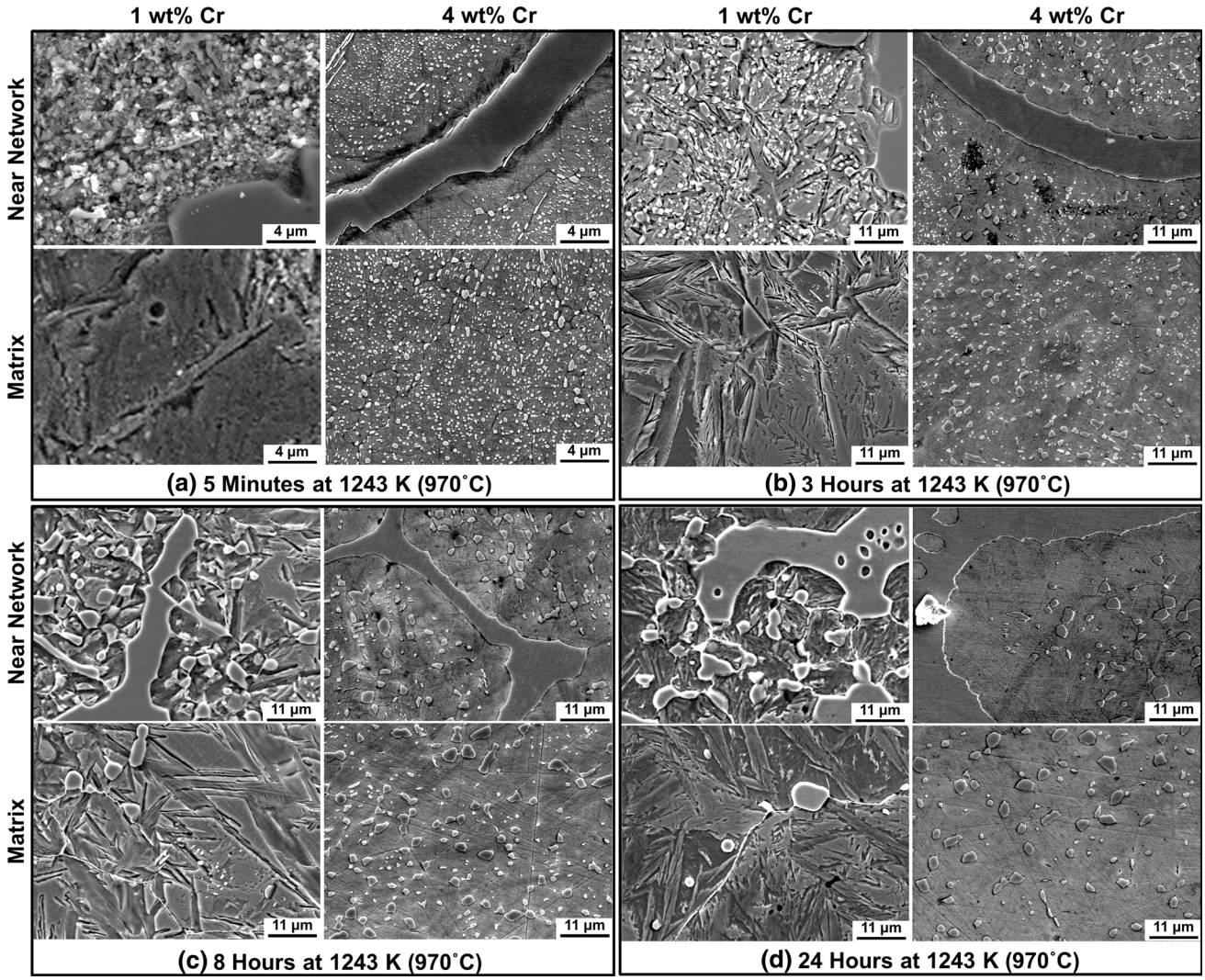

Fig. 2—SEM micrographs of microstructure at locations near the network branches and in the matrix in both 1Cr and 4Cr UHCS heat treated at 1243 K (970 °C) for (*a*) 5 min, (*b*) 3 h, (*c*) 8 h, and (*d*) 24 h.

Figure 5. Table II shows the compositions of the different microstructural features in the heat-treated 1Cr and 4Cr UHCS (note that carbon contents measured from EDS are not accurate and thus were not included in Table II). The "Overall Composition" EDS measurements in Table II matched the reported chemical composition in Table I, with the exception of Mo. This was attributed to the sampling of MnS inclusions during the area scans. It is well known that EDS peaks of Mo and S overlap and the peaks were not deconvoluted. Sampling of inclusion particles like MnS was avoided as much as possible when making the point EDS measurements. The Cr content of the network, matrix, and particles in the 1Cr UHCS was roughly one-fourth that of the 4Cr UHCS. The Mo content of cementite in the 1Cr UHCS was higher than the 4Cr UHCS. The EDS measurements were consistent with calculations in Thermo-Calc indicating that cementite in the 1Cr UHCS should contain less Cr and more Mo than in the 4Cr UHCS.

B. *OM*

Topographical contrast between matrix and particles was very poor in SEM images of the 1Cr UHCS, and consequently particle sizes could not be determined from SEM micrographs of the 1Cr UHCS. However, cementite appeared very bright and pearlite appeared very dark in the OM micrographs, such that contrast between cementite and matrix was much stronger in OM images.

OM micrographs of 1Cr UHCS samples heat treated at 1043 K (800 °C) are shown in Figure 6. Some particles could be resolved in the OM micrographs after 15 to 90 minutes of heat treating at 1043 K (800 °C). The OM images indicated clustering of particles around the network branches, but the areas further away from the network still contained many cementite particles. OM micrographs of low Cr UHCS heated treated at 1173 K (900 °C) for duration of 5 minutes to 24 hours are shown in Figure 7. Particles first became resolvable between 5 and 15 minutes of heat treatment at 1173 K

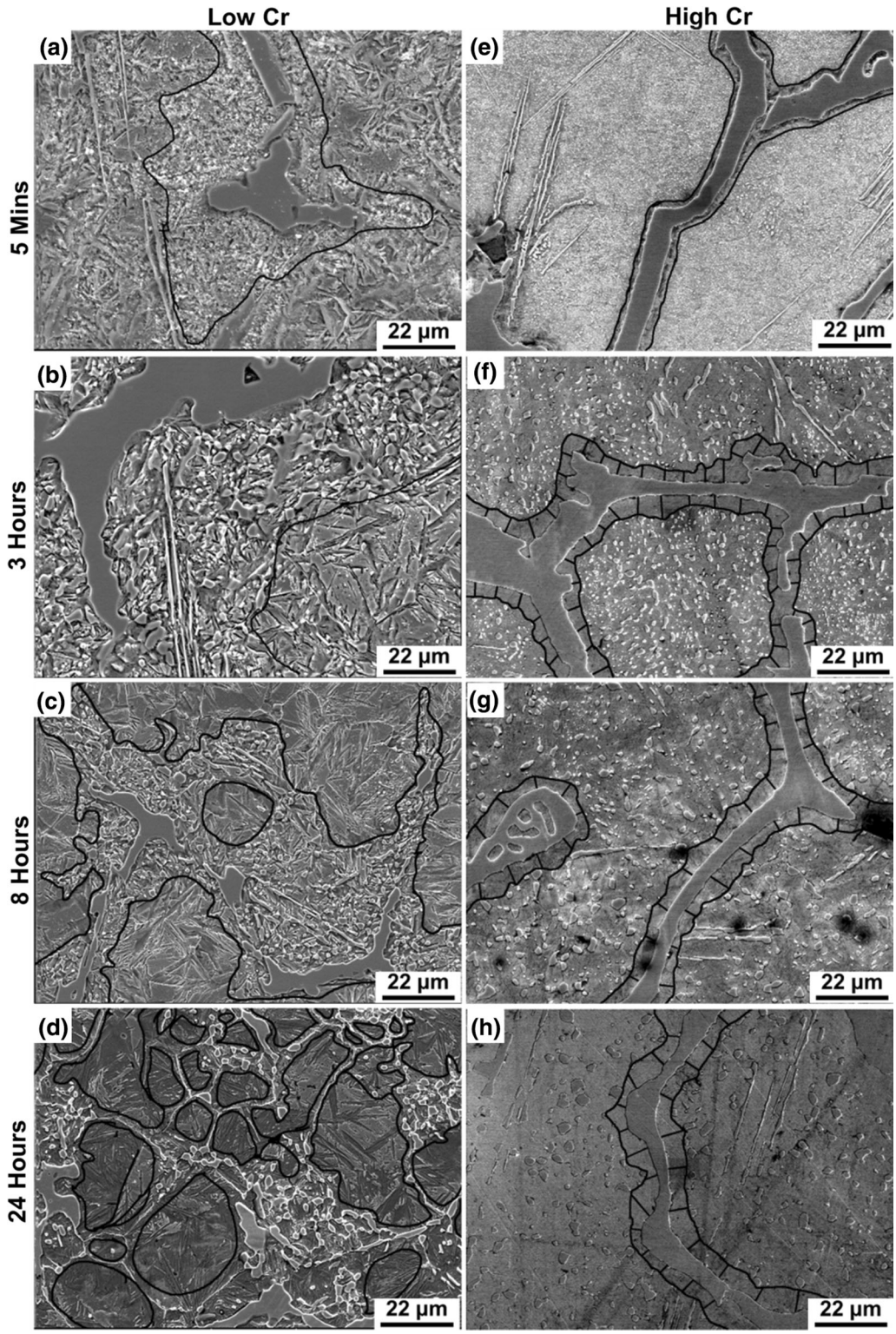

Fig. 3—SEM micrographs of the (*a* through *d*) 1Cr and (*e* through *h*) 4Cr UHCS after heat treatments of 5 min through 24 h at 1243 K (970 °C) at locations near the network branches. Dark lines drawn manually onto the micrographs denote boundaries between regions which contain many particles and regions which were mostly particle free.

(900 °C). Once again, clustering of particles near network branches was evident in the micrographs. A series of OM micrographs of the 1Cr UHCS heated treated at 1243 K (970 °C) for times of 5 minutes to 8 hours are shown in Figure 8. Some particles could already be resolved in OM micrographs after 5 minutes of heat treatment. Particle clustering was again evident near network branches; however, it appeared that areas of the matrix further away from the network branches were entirely devoid of particles.

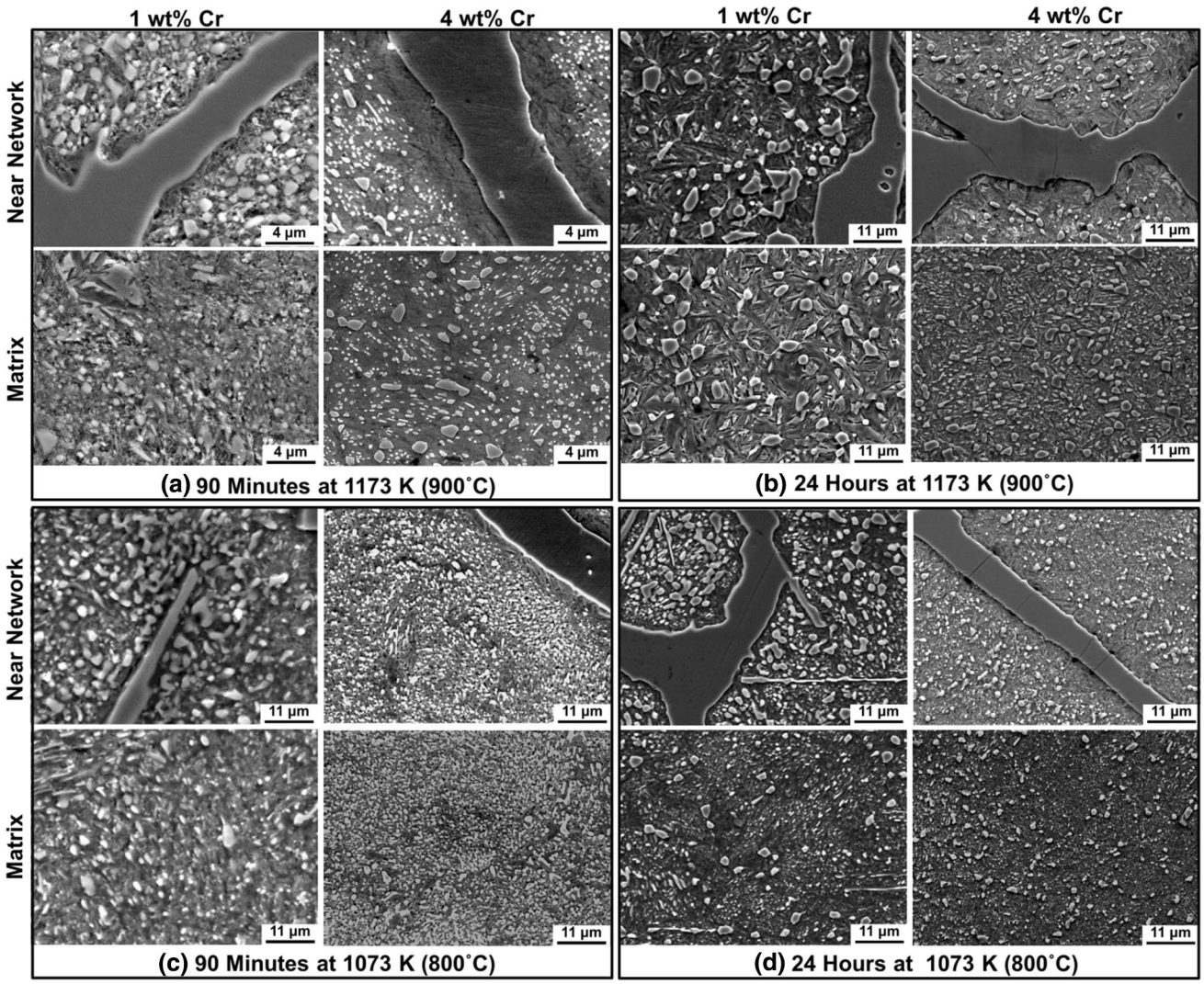

Fig. 4—SEM micrographs of microstructure at locations near the network branches and in the matrix in both 1Cr and 4Cr UHCS heat treated at (*a*) 1173 K (900 °C) for 90 min, (*b*) 1173 K (900 °C) for 24 h, (*c*) 1073 K (800 °C) for 90 min, and (*d*) 1073 K (800 °C) for 24 h.

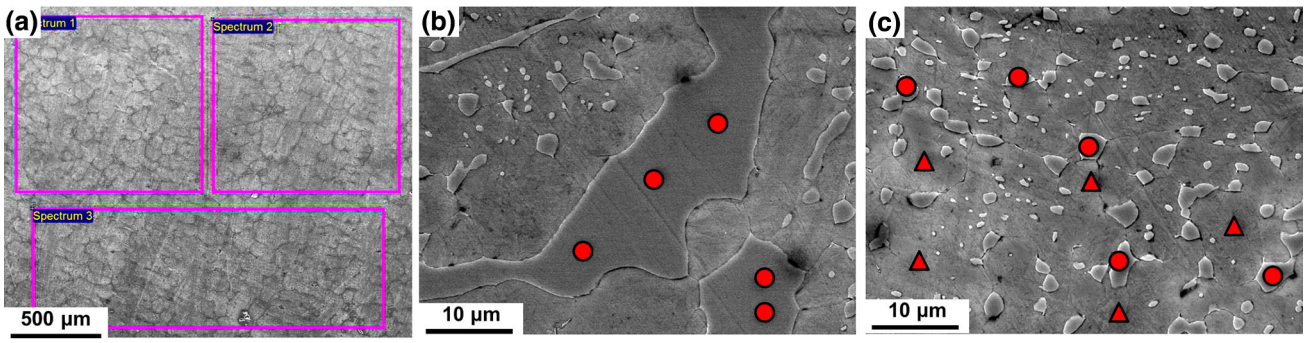

Fig. 5—EDS scan locations indicated on SEM micrographs of 4Cr UHCS measuring composition of (*a*) the entire microstructure, (*b*) the cementite network, and (*c*) cementite particles (circles) and matrix (triangles).

C. *Particle Sizes*

Figure 9 shows particle size data as a function of time and temperature for the 1Cr UHCS. In our previous study of particle coarsening in 4Cr UHCS,[14] particle size distributions were found through analysis of SEM images. The methodology used to analyze particle sizes in the 4Cr UHCS was not suitable for SEM images of the 1Cr UHCS due to poor particle/matrix contrast. Instead, OM micrographs such as those shown in Figures 6, 7, and 8 were analyzed to measure particle sizes. The minimum particle size that could be resolved

in the OM micrographs was about ~ 0.4 μm in diameter, whereas particles of 0.06 μm diameters were resolvable in SEM micrographs. It should also be noted that the 1Cr particle sizes were measured in the vicinity of network branches where clustering of particles occurred, while the 4Cr particle sizes were measured away from the network branches to avoid the denuded zones. Thus, no direct comparison of particle sizes *vs* time is made between the 1Cr and 4Cr UHCS.

Table II. Compositions (in Wt Pct) of Different Phases Within the Heat-Treated 1Cr and 4Cr UHCS Measured Using EDS

Overall Composition	Meas.	Fe	Cr	Mn	Mo	Si	Ni
1Cr UHCS	3	84	0.9	0.7	0.6	0.7	1.2
4Cr UHCS	3	88	4.4	0.9	0.6	0.8	1.5
Matrix Composition	Meas.	Fe	Cr	Mn	Mo	Si	Ni
1Cr UHCS	3	88	0.6	0.6	0.4	1.0	1.4
4Cr UHCS	5	92	2.8	0.7	0.3	0.9	1.7
Network Composition	Meas.	Fe	Cr	Mn	Mo	Si	Ni
1Cr UHCS	5	87	3.6	1.3	1.5	0.1	0.3
4Cr UHCS	5	76	14.5	1.2	0.8	0.1	0.3
Particle Composition	Meas.	Fe	Cr	Mn	Mo	Si	Ni
1Cr UHCS	5	84	3.3	1.2	1.1	0.2	0.3
4Cr UHCS	5	79	12.0	1.2	0.6	0.1	0.4

IV. DISCUSSION

A. *Particle Size Trends*

One of the purposes of this study was to investigate whether the Cr in the 4Cr UHCS was responsible for lowering the effective diffusion coefficient for cementite coarsening to inhibit volumetric diffusion. Depending on the heat-treatment time and temperature, the IG distribution in the 4Cr UHCS was typically centered at sizes smaller than 0.4 μm.[14] Due to the resolution limits in the OM, it was not possible to separate a potentially multimodal particle distribution in the 1Cr UHCS into its component intragranular (IG) and grain boundary (GB) distributions. IG particles tend to be smaller and would be underrepresented in the final particle size distribution due to the 0.4 μm cutoff. Thus, it was not possible to quantitatively describe the kinetics of particle coarsening. However, the clustering behavior in the 1Cr UHCS indicated that lowering the Cr content had an impact on the coarsening behavior consistent with an increase in effective diffusion coefficient.

B. *Particle Clustering and Denuded Zones*

The new finding of this study is that modifying the Cr content can significantly influence the distribution of cementite in regions within a few μm of the cementite network. Reducing Cr content from 4 wt pct to 1 wt pct caused clusters of cementite to form near the cementite network instead of denuded zones. We note that Krawczyk *et al.*[28] observed no such clustering during heat treatment of a steel with a 2C-1Cr composition. The main difference in processing between the two studies was the cooling rate (samples in that study were cooled at 48 °C/min and in this study samples were

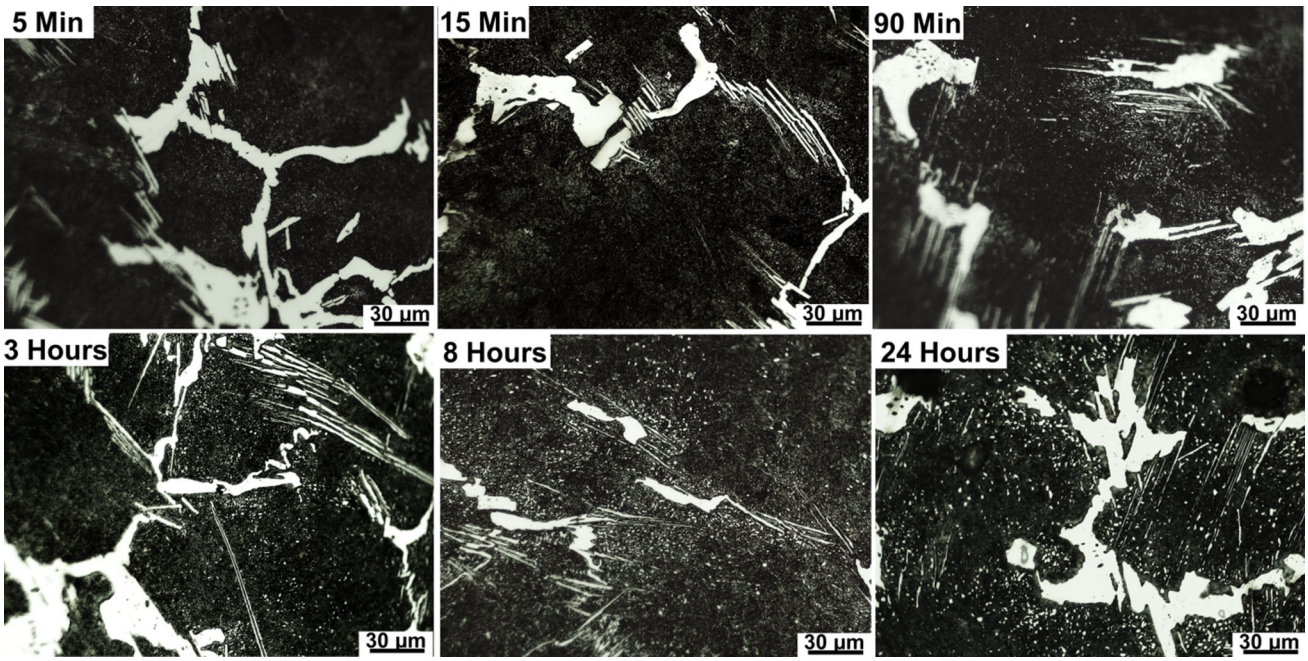

Fig. 6—OM micrographs of 1Cr UHCS microstructure near branches of the network after heat treating at 1073 K (800 °C) for 5 min to 24 h.

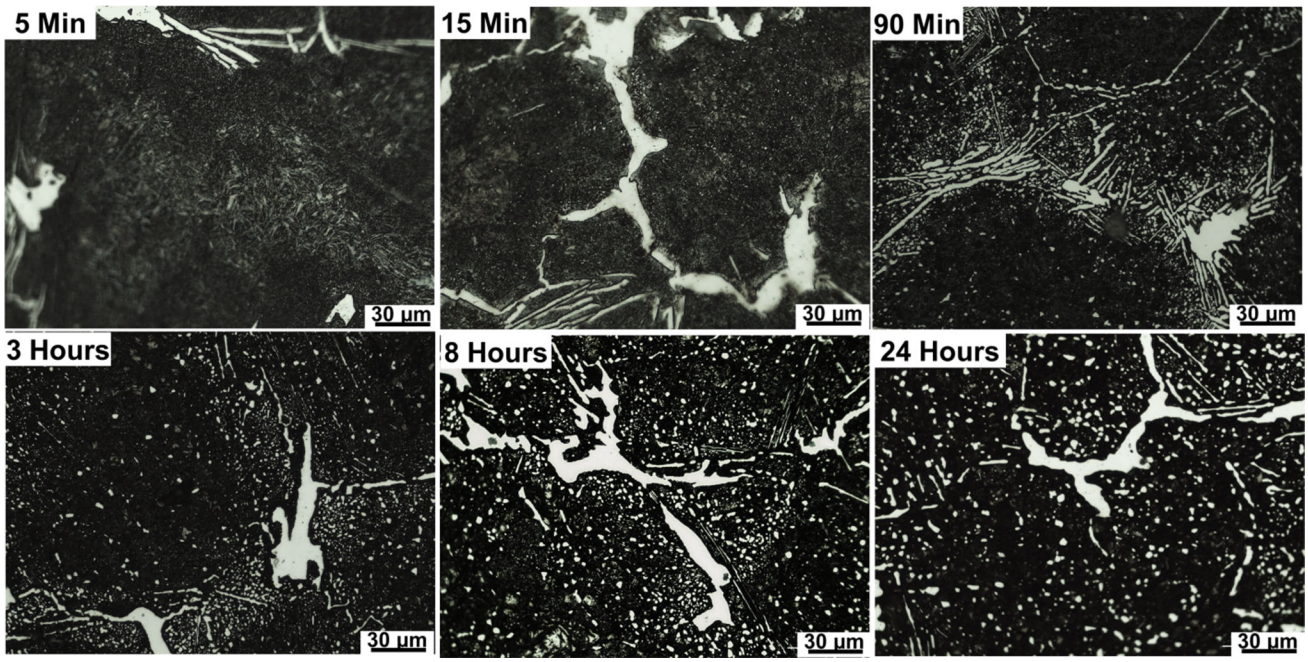

Fig. 7—OM micrographs of 1Cr UHCS microstructure near branches of the network after heat treating at 1173 K (900 °C) for 5 min to 24 h.

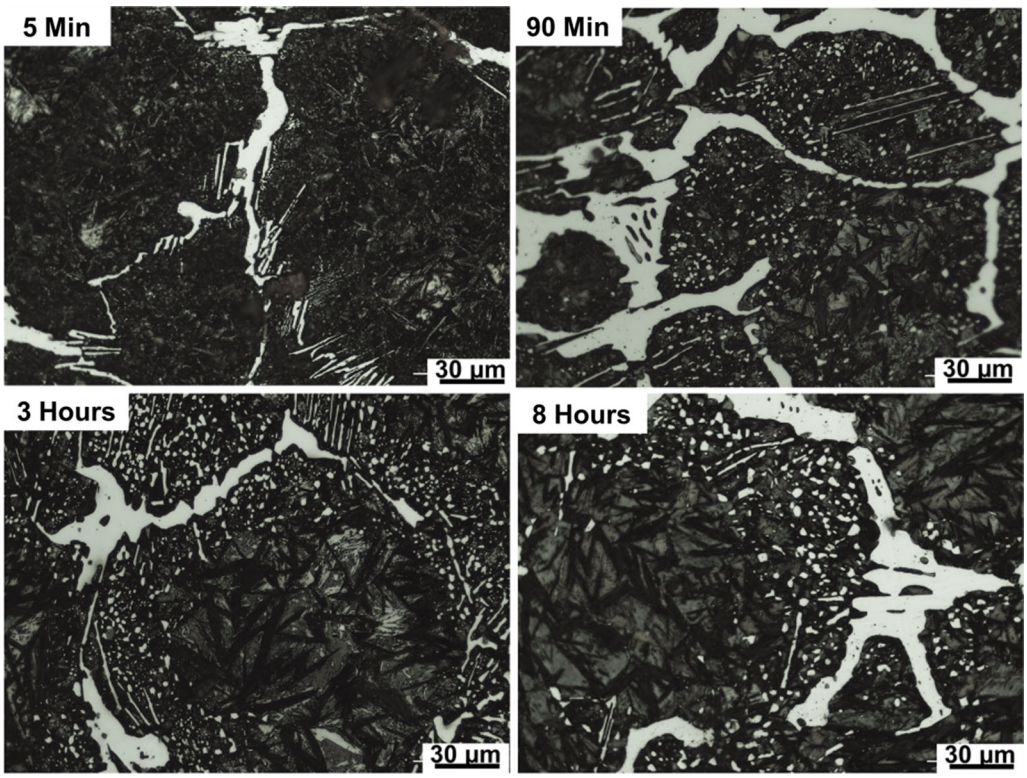

Fig. 8—OM micrographs of the low Cr UHCS microstructure near branches of the network after heat treating at 1243 K (970 °C) for 5 min to 8 h.

water-quenched). Since clustering was not observed in the water-quenched 4Cr UHCS, composition must also have played an important role in microstructural evolution during the heat treatments.

There are two possible explanations for denuded zone growth: (1) denuded zones grew because part of the network dissolved, and (2) denuded zones grew because particles near the network dissolved. Case (1) cannot be

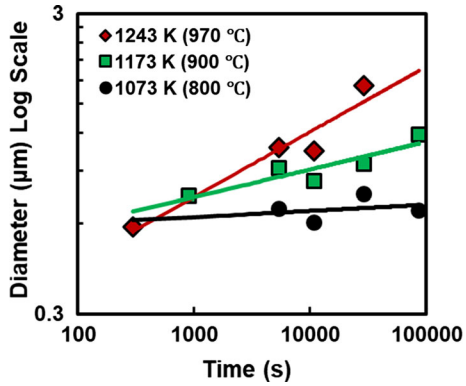

Fig. 9—Average particle diameters (> 0.4 μm) in 1Cr UHCS.

the sole cause of the denuded zones because the denuded zones in our previous study of 4Cr UHCS grew to an average of 7 μm in size on either side of network branches after 24 hours of heat treatment at 970 °C, which was larger than the average starting thickness of the network branches. In the following sections, four factors are considered that might have contributed to the development of particle clustering zones *vs* denuded zones. These are (1) the volume fractions of cementite available for particle formation, (2) the initial spacing of pearlite lamellae prior to the start of heat treatment, (3) the steepness of the concentration gradients in the microstructure, and (4) stresses developed due to mismatches in the thermal expansion coefficients of austenite and cementite.

1. *Volume fraction of spheroidizing cementite*

Figure 10 shows equilibrium volume fractions of phases in the UHCS plotted as a function of temperature (calculated in Thermo-Calc using as input the compositions shown in Table I). Dashed lines denote the heat-treatment temperatures used in this study and the corresponding cementite volume fractions. Thermo-Calc indicated that cementite and austenite were the only two stable phases during all the heat treatments. The 1Cr UHCS had an equilibrium cementite volume fraction about 0.04 lower than the 4Cr UHCS at 1043 K and 1143 K (800 °C and 900 °C), and about 0.07 lower than the 4Cr UHCS at 1243 K (970 °C).

The volume fraction of spheroidizing cementite should theoretically be equal to the cementite network volume fraction subtracted from the equilibrium cementite volume fraction, assuming that (1) the total cementite volume fraction reached equilibrium during the heat-treatment experiments; (2) cementite was present only in the particles and network; and (3) no additional cementite formed during the water quenching. Volume fractions of the cementite network were measured from OM micrographs for each heat-treated sample. Network volume fractions were subtracted from the equilibrium volume fractions of cementite to estimate the amount of cementite that spheroidized during the heat treatments, as shown in Table III. These calculations indicated that at 1243 K (970 °C) there was less cementite that could spheroidize in the 1Cr UHCS than in the 4Cr UHCS.

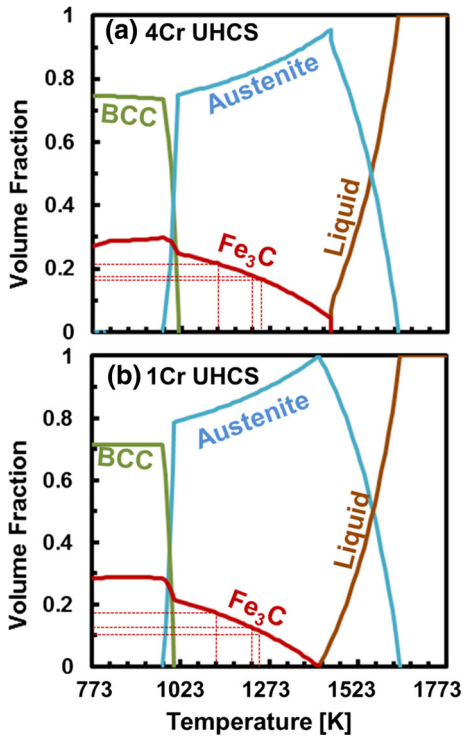

Fig. 10—Equilibrium volume fractions of the phases in (*a*) 4Cr and (*b*) 1Cr UHCS (from Thermo-Calc). Dotted lines indicate equilibrium cementite volume fractions at 1043 K, 1143 K, and 1243 K (800 °C, 900 °C, and 970 °C).

However, the amount of cementite available for particle formation was similar in the 1Cr and 4Cr UHCS at lower heat-treatment temperatures. The low availability of cementite in the 1Cr UHCS at 1243 K (970 °C) could explain the absence of particles in the matrix away from the cementite network branches. If coarsening of particles closer to the cementite network was favored, then the particles away from the network would eventually disappear.

The amount of cementite that could spheroidize and coarsen was not likely a major contributor to clustering in the 1Cr UHCS. Clustering was observed in the 1Cr UHCS both at lower temperatures (when the amount of spheroidizing cementite was comparable to that of the 4Cr UHCS), and at higher temperatures (when the amount of spheroidizing cementite was lower). Cementite particles showed a strong preference for clustering near network branches, such that the matrix became devoid of particles when cementite availability was low. Thus, particle clustering near network branches appeared to be favored in the 1Cr UHCS. There are two possible explanations for denuded zone growth: (1) Denuded zones grew because part of the network dissolved, and (2) denuded zones grew because particles near network dissolved.

2. *Lamellar spacing prior to heat treatment*

Pearlite inter-lamellar spacing was roughly three times larger in the 1Cr UHCS than in the 4Cr UHCS. Particles initially form from spheroidization of pearlite lamellae. The lamellar spacing thus determines the initial

Table III. Cementite Available for Particle Formation at Different Temperatures

1Cr UHCS	1043 K (800 °C)	1143 K (900 °C)	1243 K (970 °C)
Equilibrium Vol. Fraction Fe_3C	0.19	0.15	0.11
− Avg. Fe_3C Network Vol. Fraction	0.10 ± 0.03	0.07 ± 0.01	0.07 ± 0.02
= Fe_3C for Particles	0.09 ± 0.03	0.08 ± 0.01	0.04 ± 0.02
4Cr UHCS	**1043 K (800 °C)**	**1143 K (900 °C)**	**1243 K (970 °C)**
Equilibrium Vol. Fraction Fe_3C	0.24	0.20	0.18
− Avg. Fe_3C Network Vol. Fraction	0.12 ± 0.03	0.12 ± 0.01	0.09 ± 0.02
= Fe_3C for Particles	0.12 ± 0.03	0.08 ± 0.01	0.09 ± 0.02

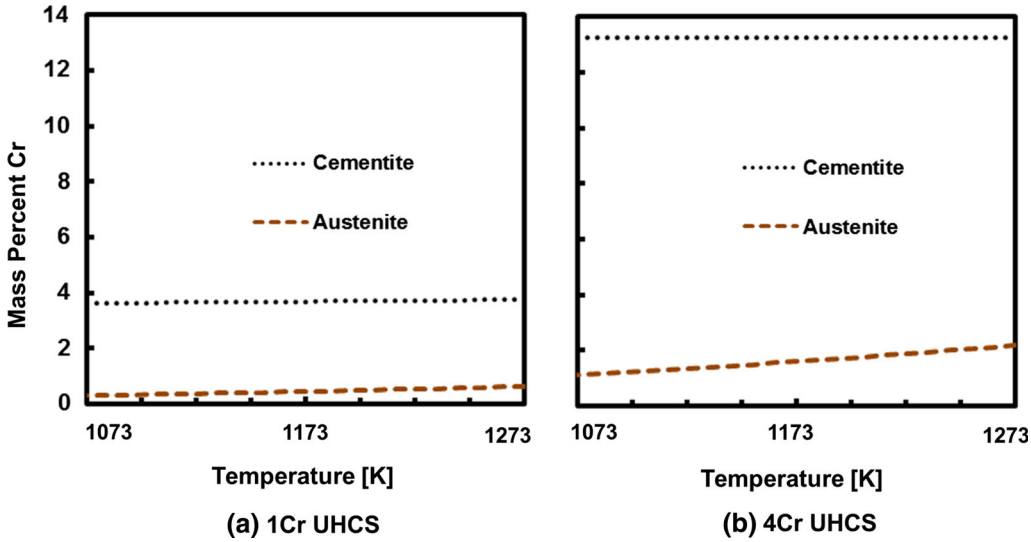

Fig. 11—Equilibrium Cr contents in cementite and austenite calculated in Thermo-Calc for (*a*) the 1Cr UHCS and (*b*) the 4Cr UHCS.

separation of particles from each other at the start of spheroidization. Thus, it is possible that larger inter-lamellar spacing contributed to the lower particle spatial density away from the network in that in the 1Cr UHCS. However, greater inter-lamellar spacing may be ruled out as a cause of the clustering near the network in the 1Cr UHCS, since a larger initial particle separation could not possibly lead to the observed clustering behavior.

3. *Concentration gradient towards network*

The observation of clustering instead of denuded zones in the 1Cr UHCS could be attributed to a concentration gradient in the UHCS. According to the Gibbs–Thomson equation, solute concentration at particle/matrix interfaces is increased by higher curvature and by higher matrix solute concentration. Particles have very high radii of curvature (1 μm or less) compared to branches of the cementite network, which are essentially flat. In our previous study,[14] we hypothesized that the denuded zones near the network carbides in 4Cr UHCS were caused by a concentration gradient of Cr and/or C directed towards the low-curvature cementite network. Particle curvature should be similar in both the 1Cr and 4Cr UHCS since the particle sizes are comparable. The difference in Cr content should thus affect only the matrix solute concentration term in the Gibbs–Thomson equation.

Figure 11 shows that the equilibrium Cr content in the matrix and cementite was higher by a factor of 3 to 4 in the 4Cr UHCS compared to the 1Cr UHCS (in agreement with EDS measurements in Table II). The solute concentration at the matrix/particle interfaces would thus be about four times higher in the 4Cr UHCS. This difference in solute concentration would have affected the steepness of the concentration gradient, and might be a factor contributing to the different clustering/denuded zone phenomena in the 1Cr and 4Cr.

4. *Coefficients of thermal expansion*

Another factor that might have influenced diffusivity was stress developed during heating due to mismatched thermal expansion coefficients of cementite and austenite. Volumetric thermal expansion of cementite and austenite were calculated in Thermo-Calc for a UHCS containing 2 wt pct C and variable amounts of Cr. Figure 12(a) shows the volumetric thermal expansion coefficient of austenite and cementite (α) as a function of Cr content at 1243 K (970 °C). Figure 12(b) shows the ratio of the thermal expansion coefficients of cementite

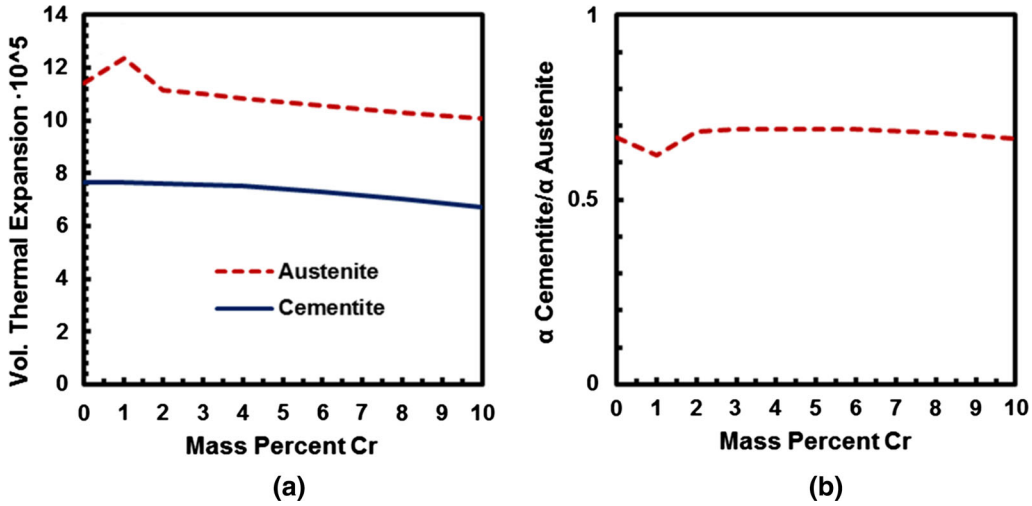

Fig. 12—Variation with Cr content of (*a*) volumetric thermal expansion coefficients of austenite and cementite and (*b*) the ratio of the cementite and austenite coefficients at 1243 K (970 °C) (from Thermo-Calc).

and austenite at 1243 K (970 °C). The thermal expansion of austenite peaked at about 1wt pct Cr, while the expansion of cementite only changed slightly with Cr content. The net result was that the mismatch in thermal expansion coefficients of austenite and cementite was about 11 pct higher for the 1Cr UHCS than for the 4Cr UHCS. Thus, in the present study, the 1Cr UHCS would have experienced a larger compressive stress during heating. It is difficult to predict the effects of stress on diffusivity in a given system,[29] but others have shown that increased compressive stress led to increased self-diffusivity in ferrite[30] and increased interstitial diffusivity in austenite.[31] The higher thermal stress and/or diffusivity may also have contributed to the clustering behavior observed in the 1Cr UHCS.

C. *Implications of This Study*

Clustering is likely deleterious to steel mechanical properties—both wear resistance and toughness might be negatively impacted. Wear resistance might suffer due to an uneven carbide particle resulting in hard and soft spots in the steel, and toughness might suffer due to the clustered particles providing many additional sites for crack initiation near the network. Thus, steelmakers are advised to exercise caution when spheroidizing UHCS with Cr contents below 4 wt pct. In the case that clustering is observed in the microstructure, the severity of the phenomenon might be reduced by lowering the heat-treatment time, temperature, or by increasing the Cr content of the alloy.

V. CONCLUSIONS

In this study, an initially pearlitic 2C-1Cr UHCS was heat treated at 1043 K, 1143 K, and 1243 K (800 °C, 900 °C, and 970 °C), comparison with a 2C-4Cr UHCS studied previously. Averaging over all three temperatures, sizes of particles in the 1Cr UHCS were 300 pct larger than particles 4Cr UHCS after 5 minutes of heat treatment, and 10 pct larger after 25 hours of heat treatment, indicating that lowering the Cr content increased the effective diffusivity during coarsening. Cementite particles in the 1Cr UHCS clustered in zones of up to 20 μm from network branches in contrast to the 4Cr UHCS, which exhibited denuded zones of up to 8 μm from network branches.

Four conclusions can be made regarding possible contributors to clustering and denuded zones:

(1) The volume fraction of cementite available for particle formation did not determine whether clustering or denuded zones occurred.
(2) Differences in pearlite inter-lamellar spacing did not directly cause clustering, since spacing in the 1Cr UHCS was roughly three times than in the 4Cr UHCS.
(3) Higher Cr content increased the steepness of the concentration gradient in UHCS. The steepness of the concentration gradient may have influenced whether denuded zones or particle clusters formed near branches of the cementite network.
(4) According to calculations in Thermo-Calc, the mismatch in thermal expansion coefficient between austenite and cementite was about 11 pct higher in the 1Cr UHCS than in the 4Cr UHCS. The increased stress due to the mismatch may have contributed to the clustering phenomenon observed in the 1Cr UHCS.

ACKNOWLEDGMENTS

The authors appreciate Miller Centrifugal Casting for providing the mill roll parts for this study. This project was financed in part by a Grant from the Commonwealth of Pennsylvania Department of Community and Economic Development (DCED),

Developed in PA Program (D2PA). Funding support is also acknowledged from the National Science Foundation, CMMI Award No. 1436064. The authors acknowledge use of the Materials Characterization Facility at Carnegie Mellon University supported by Grant MCF-677785 as well as helpful discussions with Professor Chris Pistorius of Carnegie Mellon University.

REFERENCES

1. United States Patent, 3951697, 1976.
2. B. Walser and O.D. Sherby: *Metall. Trans. A*, 1979, vol. 10A, pp. 1461–71.
3. D. Lesuer, C. Syn, and O. Sherby: in *SAE Technical Paper 960314*, SAE International Congress and Exposition, 1996.
4. D.R. Lesuer, C.K. Syn, A. Goldberg, J. Wadsworth, and O.D. Sherby: *JOM*, 1993, vol. 45, pp. 40–46.
5. I.M. Lifshitz and V.V. Slyozov: *J. Phys. Chem. Solids*, 1961, vol. 19, pp. 35–50.
6. C. Wagner: *Zeitschrift für Elektrochemie*, 1961, vol. 65, pp. 581–91.
7. M.V. Speight: *Acta Metall.*, 1968, vol. 16, pp. 133–35.
8. A.J. Ardell: *Acta Metall.*, 1972, vol. 20, pp. 601–09.
9. B.A. Lindsley and A.R. Marder: *Acta Mater.*, 1998, vol. 46, pp. 341–51.
10. S.P. Rawal and J. Gurland: *Metall. Trans. A*, 1977, vol. 8A, pp. 691–98.
11. C.K. Syn, D.R. Lesuer, and O.D. Sherby: *Metall. Mater. Trans. A*, 1994, vol. 25A, pp. 1481–93.
12. J.D. Verhoeven and E.D. Gibson: *Metall. Mater. Trans. A*, 1998, vol. 29, pp. 1181–89.
13. *Rolls for the Metalworking Industries*, 2nd ed., Gene.E. Lee, ed., *Rolls for the Metalworking Industries*, Iron and Steel Society, Warrendale, PA, 2002.
14. M.D. Hecht, Y.N. Picard, and B.A. Webler: *Metall. Mater. Trans. A*, 2017, vol. 48A, pp. 2320–35.
15. A.A. Vasilyev, S.F. Sokolov, N.G. Kolbasnikov, and D.F. Sokolov: *Phys. Solid State*, 2011, vol. 53, pp. 2194–2200.
16. G.H. Zhang, J.Y. Chae, K.H. Kim, and D.W. Suh: *Mater. Charact.*, 2013, vol. 81, pp. 56–67.
17. P. Deb and M.C. Chaturvedi: *Metallography*, 1982, vol. 354, pp. 341–54.
18. A.R. Marder and B.L. Bramfitt: *Metall. Trans. A*, 1975, vol. 6A, pp. 2009–14.
19. W.J. Nam and C.M. Bae: *Scr. Mater.*, 1999, vol. 41, pp. 313–18.
20. A.M. Cree, R.G. Faulkner, and A.T. Lyne: *Mater. Sci. Technol.*, 1995, vol. 11, pp. 566–71.
21. Z.Q. Lv, S.H. Sun, Z.H. Wang, M.G. Qv, P. Jiang, and W.T. Fu: *Mater. Sci. Eng. A*, 2008, vol. 489, pp. 107–12.
22. R.V. Day and J. Barford: *Nature*, 1968, vol. 217, pp. 1145–56.
23. F.S. Birks, N. Meier, and G.H. Pettit: *Introduction to the High Temperature Oxidation of Metals*, 2nd ed., Cambridge University Press, Cambridge, 2006.
24. G.F. Vander Voort and A. Roósz: *Metallography*, 1984, vol. 17, pp. 1–17.
25. C.A. Schneider, W.S. Rasband, and K.W. Eliceiri: *Nat. Methods*, 2012, vol. 9, pp. 671–75.
26. S.A. Saltikov: *Proc. 2nd Int. Cong. Stereol.*, H. Elias, ed., Springer-Verlag New York Inc., Chicago, 1967, pp. 163–73.
27. D.L. Sahagian and A.A. Proussevitch: *J. Volcanol. Geotherm. Res.*, 1998, vol. 84, pp. 173–96.
28. J. Krawczyk, R. Dziurka, and E. Rożniata: *Metall. Foundry Eng.*, 2008, vol. 34, p. 125.
29. M.J. Aziz: *Defect. Diffus. Forum*, 1998, vols. 153–155, pp. 1–10.
30. F.S. Buffington and M. Cohen: *J. Met.*, 1952, vol. 4, pp. 859–60.
31. T.L. Christiansen and M.A.J. Somers: *Defect Diffus. Forum*, 2010, vols. 297–301, pp. 1408–13.